

# Prompt Generation Networks for Input-based Adaptation of Frozen Vision Transformers

Jochem Loedeman<sup>1</sup>, Maarten C. Stol<sup>2</sup>, Tengda Han<sup>3</sup>, Yuki M. Asano<sup>1</sup>

<sup>1</sup> VIS Lab, University of Amsterdam, <sup>2</sup> BrainCreators, <sup>3</sup> VGG, University of Oxford

j.m.loedeman@gmail.com, htd@robots.ox.ac.uk, y.m.asano@uva.nl

## Abstract

*With the introduction of the transformer architecture in computer vision, increasing model scale has been demonstrated as a clear path to achieving performance and robustness gains. However, with model parameter counts reaching the billions, classical finetuning approaches are becoming increasingly limiting and even unfeasible when models become hosted as inference APIs, as in NLP. To this end, visual prompt learning, whereby a model is adapted by learning additional inputs, has emerged as a potential solution for adapting frozen and cloud-hosted models: During inference, this neither requires access to the internals of models' forward pass function, nor requires any post-processing. In this work, we propose the Prompt Generation Network (PGN) that generates high performing, input-dependent prompts by sampling from an end-to-end learned library of tokens. We further introduce the "prompt inversion" trick, with which PGNs can be efficiently trained in a latent space but deployed as strictly input-only prompts for inference. We show the PGN is effective in adapting pre-trained models to various new datasets: It surpasses previous methods by a large margin on 12/12 datasets and even outperforms full-finetuning on 5/12, while requiring 100x less parameters.*

## 1. Introduction

Large-scale pretrained models, such as those obtained from self-supervised or vision-language pretraining have shown remarkable performance gains for various visual tasks. Particularly models such as SEER [16], CLIP [38] and ALIGN [24] have demonstrated that large and multi-modal datasets can yield models that exhibit novel abilities in terms of robustness or few- and zero-shot learning. However, the requirements in terms of dataset size and compute infrastructure are exceedingly prohibitive for most researchers, such that these models are and will likely remain limited in terms of their diversity and availability. Exacerbating this trend further, model sizes are steadily increas-

ing: a case in point is the recent development of a Vision Transformer model with 22B parameters [11]. Eventually, models will reach sizes that can only be served via dedicated hardware or API interfaces, as is already the case for the largest and best models in NLP (e.g. GPT-3 [4]).

Both of these developments mean that many classic approaches for finetuning models are not applicable anymore. This is because the prevailing paradigms entangle the adaptation and computation phase, for example by directly adapting weights in a model or by requiring internal access to the model's forward pass and modifying it with additional inputs [24], or additional intermediate layers [53].

A solution to this is adapting frozen models by solely learning additional inputs. This approach covers not only the setting where the model is impossible to directly change, e.g. because it is served via an API or hard-coded as an application-specific integrated circuit (ASIC), but also where it is very sensitive to changes, e.g. due to quantization. Additionally learned inputs, also called *prompts* are typically learned per domain and downstream task and have shown promising results for adapting to image domains [2] and are broadly inspired from adversarial reprogramming [14, 28]. However, so far, the resulting performances have fallen short compared to finetuning models.

In this paper, we argue that the main reason for this shortfall is the arbitrary definition of a domain and the resulting limited modeling flexibility, as the same prompts are always added as inputs, regardless of datum. In contrast, we propose a new method that allows adapting to *every single* input image. For this, we introduce the Prompt Generation Network (PGN) that learns to generate new prompts for every image by combining items from a commonly learned library of tokens. Furthermore, as these prompts' purpose is to only aid the large-scale model, the PGN can be kept lightweight, which allows for efficient, yet strong modelling capabilities. By fully decoupling the adaptation part from the internal model computations, a PGN can be simply deployed on client devices after an initial stage of server-side training. On a benchmark covering 12 datasets, we show that our PGN approach achieves performances that

matches and outperforms those of fully finetuned models, while being two orders of magnitude more efficient in terms of additional parameters. This demonstrates that our proposed method effectively closes the divide between high-performing classical finetuning and previously constrained adaptation of frozen vision models.

Overall, this paper makes four main contributions:

- We develop a simple and effective framework for learning input-dependent visual prompts via Prompt Generation Networks.
- We propose an alternative inference mode that decouples the PGN from the large-scale model, such that it is possible to arrange them in a client-server setup, making our approach compatible with recent developments in the industry.
- We demonstrate the generalizability and state-of-the-art performances of the proposed method across 12 datasets, architectures and settings such as multi-dataset inference.
- Finally, via quantitative and qualitative analyses, we showcase how with our method a “division of labor” emerges between the frozen model and the PGN.

## 2. Related Works

### 2.1. Large-scale pretrained models

**Multi-modal Pretraining.** Most modern works in vision-language modeling are inspired by the recent trend of large-scale pretraining, involving data-hungry transformer architectures [43] fed by web-scale datasets. Two recent approaches are CLIP [38] and ALIGN [24], which use a contrastive objective to jointly optimize an image and text encoder to align the embeddings and are trained on datasets with hundreds of millions of image-text pairs.

**Visual-only Pretraining.** Another source for obtaining strong visual encoders is to utilize large-scale supervised datasets such as JFT [11] or apply self-supervised learning on visual inputs. For the latter, a pretext task such as clustering [1, 6], contrastive discrimination [8, 18, 48] or teacher-based distillation [7] is used to train on large datasets without any annotations. However, for both approaches, the amount of compute and, or, dataset size required are tremendous, making the adaption of such models increasingly important.

### 2.2. Adaptation Methods

While pretrained vision models generally need to be finetuned, vision-language models can perform zero-shot transfer by prompting the text encoder to perform downstream tasks. However, for most datasets there is still a significant performance gap with respect to full-finetuning,

which is computationally expensive and reduces robustness [47]. A range of alternative methods has been proposed to address these issues.

**Adapters and partial finetuning.** Inspired by previous works in NLP [23, 37], lightweight feature adapters (made of trainable parts in between frozen ones) have shown performance gains [15, 53]. Requiring few additional parameters, only finetuning the bias parameters of pretrained models has also been proposed [5, 51]. In contrast, VPT [25] learns additional inputs to multiple layers in a pretrained vision transformer [13] but also finetunes a linear classifier on top. Another finetuning-based approach proposed in [47] is to ensemble the weights between zero-shot and finetuned models and [52] which trains additional networks that are fused via summation. Specific to vision-language models, [54] learn an adaptation network between CLIP’s vision and text encoders. Although these works show promising results, they either change the underlying model’s weights or require access to the internals of the model’s forward pass for inserting additional computations. This is a key difference to our work, in which we strictly separate the adaption stage from the frozen model computation stage.

**Input-only adaptation** Optimizing solely in the *input-space*, prompt learning originates from language modeling and is a lightweight approach to adapting a model to perform downstream tasks [4, 33, 39]. For computer vision, initial efforts focused on learning continuous prompts (as opposed to prompt sentences/words) for the text encoder of pretrained vision-language models for image [50, 55] and video tasks [27]. In contrast to these, our method does not rely on multi-modal systems or a general text encoder but can be used for any visual encoder.

Most related to our work is the work of [2], that proposes visual prompting through the addition of learnable pixels, effectively learning prompts in the data space. This is the same setting as adversarial reprogramming [14, 28], where pretrained CNNs are repurposed to classify images from different datasets by applying transformations *only to the input*. This form of adaptation therefore does not affect the model itself, making it an excellent option for scenario’s with restricted model access during inference.

And although these works show significant gains, they do not match the performance of classic adaptation techniques like finetuning and linear probing. Our method bridges the performance gap by learning prompts that, unlike previous works, are adapted to each image.

## 3. Methods

The key idea of our method is to generate input-dependent visual prompts that benefit the domain adaptation process. In this section, we first briefly review the recent prompt learning methods in Section 3.1, then introduce

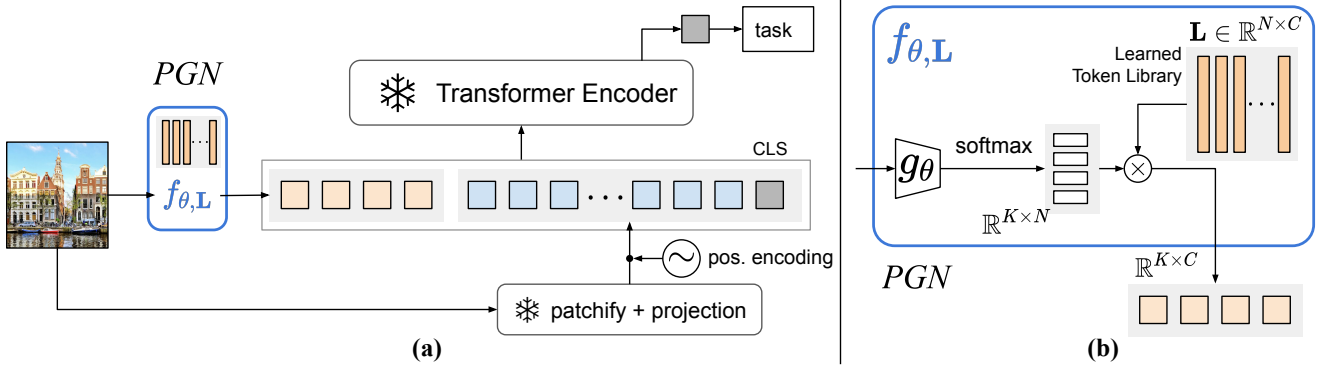


Figure 1: We propose the **Prompt Generation Network (PGN)**, a simple yet effective method that generates prompts conditioned on the input images that benefits the domain adaptation process, while keeping the whole pretrained transformer frozen. **(a)**: the overall learning pipeline including PGN, denoted by  $f_{\theta, L}$ : the learned prompt vectors are fed into the pretrained transformer encoder together with image patches for the task or domain of interest. **(b)**: the detailed structure of PGN, a lightweight neural network  $g_{\theta}$  learns probability distributions to select prompt vectors from a Token Library  $\mathbf{L}$ .

the proposed Prompt Generator Network in Section 3.2 and the Prompt inversion in Section 3.3

### 3.1. Review of prompting learning methods

In NLP, prompt learning offers a lightweight approach to tune large-scale pretrained models for performing downstream tasks. Let  $\Phi_T(\cdot)$  denote the pretrained language model and  $\mathbf{x}_T = [a_1, a_2, \dots, a_n]$  denote the input language tokens. Traditionally, the model is trained to produce a latent language embedding for the given input as  $\mathbf{z}_T = \Phi_T(\mathbf{x}_T; \text{CLS})$ , where ‘;’ denotes concatenation and CLS is the special token for classification. The latent embedding  $\mathbf{z}_T$  can be used for downstream tasks. In order to adapt the model on different tasks or different datasets, one would have to finetune the large-scale pretrained model  $\Phi_T$ , which is potentially very resource demanding and could be infeasible for models with billions of parameters.

As its name suggests, prompt learning provides a set of learnable vectors  $\mathbf{h}_T = [h_T^1, \dots, h_T^k]$  called prompt vectors, that are fed to the pretrained model and encourage it to produce desirable outputs. Formally, the prompt learning process can be written as

$$\hat{\mathbf{z}}_T = \Phi_T(\mathbf{h}_T; \mathbf{x}_T; \text{CLS}), \quad (1)$$

The prompted language embedding  $\hat{\mathbf{z}}_T$  can also be used for downstream tasks. Due to the flexibility of the prompt learning method, one can adapt the model on new tasks or new datasets by only training the lightweight prompt vectors  $\mathbf{h}_T$ , rather than finetuning the heavy pretrained model  $\Phi_T$ . This method was originally proposed in the NLP community [32, 33], and it was later used to prompt the language branch in pretrained visual-language models [27, 55].

Recently, the prompt learning technique has also been applied to large-scale pretrained *visual* models. Similarly, let  $\Phi_V(\cdot)$  denote the pretrained visual model – typically a variant of the Vision Transformer [13],  $\mathbf{x}_V =$

$[E(c_1), E(c_2), \dots, E(c_m)]$  denote the encoded input image patches, and  $\mathbf{h}_V = [h_V^1, \dots, h_V^k]$  denote the visual prompt vectors. Visual prompt learning can be formalized as

$$\hat{\mathbf{z}}_V = \Phi_V(\mathbf{h}_V; \mathbf{x}_V; \text{CLS}). \quad (2)$$

Within the previous works [2, 25] that apply prompt learning in this way, [25] apply these prompts deep within the internal computations of transformers, whereas those in [2] are in the pixel space.

### 3.2. Prompt Generator Network

Although learning prompt vectors brings flexibility to the pretrained model, a key limitation of the classic prompt learning method is that the prompt vectors are shared within the dataset and task. In other words, the prompt vectors are conditioned on the domain. However, what exactly constitutes a domain is somewhat arbitrary, *e.g.*, ImageNet both contains fine-grained distinctions (such as 120 different dog breeds) and very coarse ones (such as a single mushroom class). Therefore, having a single set of learned vectors for adaptation results in modeling capacity being wasted on items that might already be well encoded. In this section we introduce our Prompt Generator Network as a more flexible alternative to this.

Fig. 1 shows an overview of our method. Given the input image  $I_i \in \mathbb{R}^{3 \times H \times W}$  and the pretrained vision model  $\Phi_V$ , we first cut the image to  $s \times s$  patches  $\{c_1, c_2, \dots, c_{H' \times W'}\}$ , where  $c_j \in \mathbb{R}^{2 \times s \times s}$ ,  $H' = H/s$  and  $W' = W/s$ , and then encode with a linear layer  $E(\cdot)$ . To construct the visual inputs  $\mathbf{x}_V = [E(c_1), E(c_2), \dots, E(c_{H' \times W'})]$ . Rather than introducing a set of *shared* prompt vectors as described in Section 3.1, we propose to use a set of *input-dependent* prompt vectors. Formally, we use a function  $f(\cdot)$  to learn the dependency

$$\hat{\mathbf{h}}_V^i = f(I_i), \quad (3)$$

where the function  $f(\cdot)$  is learned by a neural network. While it is possible to directly transform the inputs continuously to the prompt vectors, in practice this results in a high number of parameters due to the fully-connected layers being proportional to the large input dimensionalities of transformers.

Instead, we propose to use a Token Library  $\mathbf{L} \in \mathbb{R}^{N \times C}$  that consists of  $N$  learnable feature vectors with channel dimension  $C$ . Compared to works that use memory [17, 30, 42], the Token Library’s purpose is not to learn characteristics of the dataset, but instead to steer the pre-trained model towards a certain dataset, therefore saving modeling capacity. The prompt generation network learns to generate  $K$  prompt vectors  $\hat{\mathbf{h}}_V^i = [\hat{\mathbf{h}}_V^{i1}, \dots, \hat{\mathbf{h}}_V^{iK}]$ , each of which is a combination of the feature vectors from the Token Library  $\mathbf{L}$ . In detail,

$$\hat{\mathbf{h}}_V^i = f_{\theta, \mathbf{L}}(I_i) = \text{Softmax}(g_{\theta}(I_i)) \cdot \mathbf{L} \in \mathbb{R}^{K \times C}, \quad (4)$$

where the function  $g_{\theta}(\cdot)$  denotes a learned mapping  $\{\mathbb{R}^{3 \times H \times W} \mapsto \mathbb{R}^{K \times N}\}$ , using a lightweight neural network parameterized by  $\theta$ . Compared to some works in continual learning [45, 46], the generated combination given by  $g_{\theta}(\cdot)$  is independent of the pre-trained representation given by  $\Phi_V$ , enabling the PGN to learn features that are optimized for its task of providing input-dependent prompts.

Finally all prompt vectors are fed into the frozen transformer encoder,

$$\hat{\mathbf{z}}_V^i = \Phi_V(\hat{\mathbf{h}}_V^i; \mathbf{x}_V^i; \text{CLS}). \quad (5)$$

The prompted visual features  $\hat{\mathbf{z}}_V^i$  act as input to a classifier for downstream classification tasks.

### 3.3. Prompt inversion for input-only prompting

So far, the prompt vectors learned by a PGN are fed to the frozen pretrained model between the initial projection layer and the transformer blocks. Yet if neither have access nor permission to modify the first layer of the transformer, *e.g.* because it is being accessed via an API or is implemented in hardware, this is problematic. In order to solve this, we use a ‘‘Prompt Inversion’’ operation, a simple mechanism that transforms the learned prompts to input RGB patches, which can be simply attached to the bottom of the incoming image. This yields the same prompting capabilities, and is compatible with the recent emergence of inference APIs. In this setup, the PGN is deployed on the client-side and sends the adapted inputs to the remotely hosted model.

Prompt inversion leverages the linearity of the first patch-projection layer and enables fast training by learning directly in prompt-space, while at the same time allowing for *input-only prompting* during inference and downstream applications. In detail, we can turn a prompt vector  $\hat{\mathbf{h}}_V^{ij}$  into



Figure 2: **Prompt Inversion for visual prompting.** At inference time, PGN prompts can be mapped to the input space to completely separate the adaptation step from the model’s internal computation. In this instance, the PGN outputs 14 prompts which can be visualized as 2 rows containing 7 prompt-patches each.

a patch by

$$\mathcal{P}_{(\hat{\mathbf{h}}_V^{ij})} = (\hat{\mathbf{h}}_V^{ij} - E_{\text{pos}})W_{\text{proj}}^{-1}$$

where  $E_{\text{pos}}$  denotes the positional embedding and  $W_{\text{proj}}^{-1}$  is the pseudo-inverse of the linear projection weight matrix. Note that this matrix needs to be computed only once as it stays frozen. The inverted prompt  $\mathcal{P}_{(\hat{\mathbf{h}}_V^{ij})} \in \mathbb{R}^{3 \times s \times s}$  is a RGB patch and can simply be appended to the input image and then served to the frozen transformer. In practice, the number of prompts is kept divisible by the patch size  $s$  to ensure that the images retain a rectangular format. An example of the result of this process for a ViT-B/32 is shown in Fig. 2 – note that for ViTs with smaller patch-sizes the additional input patches occupy much less space.

## 4. Experiments

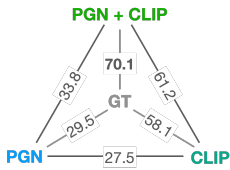
### 4.1. Implementation details

**Datasets.** In our experiments we cover 12 public image datasets: CIFAR100 & CIFAR10 [29], Oxford Flowers [35], Food101 [3], EuroSAT [20], SUN397 [49], UCF101 [41], SVHN [34], Oxford-IIIT Pets [36], DTD [10], RESISC [9] and CLEVR [26]. Out of these, we chose CIFAR100 and SUN397 for ablations in Section 4.3, as they vary in resolution, difficulty and the degree of spatial distribution of relevant image features. Please refer to Appendix for the statistics for each dataset.

**Architectures.** We use the ViT-B/32 models and use CLIP pretraining [38] obtained weights as default but compare against supervised [13] and DINO [7] self-supervised weights. The ViT weights are always kept frozen during our experiments. In the PGN, we experiment with the lightweight ResNet-based architectures [19], namely ResNet10 and ResNet18. We obtain the ResNet10 architecture by reducing the layers at each residual block from

Figure 3: **Feature similarities.**

We show the mutual information between the components and the ground-truth labels (details in Appendix). PGN learns very different embeddings to CLIP but when combined achieves strong alignment with the ground-truth labels.



	PGN backbone (alone)	CLIP	CLIP with PGN
CIFAR-100	63.7	63.1	79.3

Table 1: **Synergies.** We show performances of training our PGN’s backbone in a supervised manner against CLIP ViT-B/32 in a zero-shot manner and when combined with PGN.

ResNet18 and also reducing the depth of the first layer to only 16. Please refer to the Appendix for the details.

**Training details.** We train the PGN with a learning rate of 0.1 and apply a cosine decay learning schedule ending at zero learning rate with a linear warmup for the first 50 epochs. We use an SGD optimizer with 0.9 momentum. Except when specified, we use a batch size of 128 images on one Nvidia-1080TI GPU. Compared to the 1,000 epochs of concurrent work [2], we train our network for 500 epochs by default in Section 4.2 and 4.3 and for 1,000 in Table 4.

## 4.2. Motivation

In this section we investigate the basic feasibility of our proposed method for generating input-dependent prompts via PGNs. For this, in Table 1, we compare the results of prompting a CLIP ViT-B/32 model to correctly select the right class in a “zero-shot” manner with text-embeddings automatically generated as “This is a photo of a [class name]”. We observe that the zero-shot baseline of CLIP approximately matches that of training the network underlying the PGN in a supervised manner of around 63%. Despite this, when utilised in our method together (whereby the CLIP model’s weights are neither adapted nor interfered with in-between), the two models symbiotically increase the performance by +16% – far outperforming its isolated variants. This is further demonstrated in Fig. 3, where we compare the similarities of the representations of the various components. For this we cluster the outputs of each visual encoder (PGN, CLIP and CLIP+PGN) unsupervisedly and measure the pairwise alignment using normalised mutual information (see Appendix for details). We find that PGN+CLIP’s features are closest to the ground-truth (NMI of 70.1%) compared to both PGN (29.5%) and standalone

(a) Number of prompts.

Num.	CIFAR100	SUN397
1	75.8	68.3
4	77.8	69.6
8	77.9	<b>70.6</b>
16	<b>78.3</b>	70.0
64	77.3	68.9

(b) Size of the token library.

Size	CIFAR100	SUN397
8	75.3	69.0
16	76.4	69.6
64	77.9	<b>70.6</b>
256	78.4	<b>70.6</b>
1024	<b>78.6</b>	69.9

(c) PGN backbone.

Model (resolution)	CIFAR100	SUN397
IIP	72.1	69.6
MLP (10×10)	73.5	69.6
ResNet10 (64×64)	77.9	<b>70.6</b>
ResNet10 (224×224)	<b>79.3</b>	<b>70.6</b>
ResNet18 (224×224)	<b>79.3</b>	69.6

Table 2: **Ablations** for our PGN method. We vary the number of prompts provided to the frozen model, the size of the Token Library and the PGN backbone. Default settings are in gray.

CLIP (58.1%), in line with later results of Table 4. The low performance of only the PGN also demonstrates that it is not doing the “heavy-lifting”, as its outputs are least aligned to the ground-truth labels. Instead, PGN and CLIP’s outputs share the lowest similarity of only 27.5%. The superior performance of the combined model there results from the PGN learning features that are quite dissimilar and therefore more informative to the frozen CLIP model.

## 4.3. Ablation Studies

Next, we ablate and analyze the various choices of the PGN architecture and setting. We conduct ablation studies on CIFAR100 and SUN397 in Table 2. Unless otherwise stated, we learn 8 prompts and a Token Library of size 64 to speed up computations.

**Number of Prompts.** In Table 2a, we vary the number of prompts that the PGN generates. We find that increasing the number of prompts generally yields a better performance. Yet, the gains decrease when moving beyond 4 prompts. This shows that even a modest number of 4-8 additional tokens – when added to the 49 spatial plus 1 CLS token – can yield significant benefits.

**Token Library Size.** Next, in Table 2b, we compare the size of the Token Library’s number of items. We find that larger Token Library generally leads to better performance, although no further improvement is observed beyond 256 tokens. We conjecture the additional library items beyond 256 tokens only learn redundant information and therefore do not benefit the performance.

**Architectures.** In Table 2c, we ablate the backbone used for the PGN with input-independent prompts (IIP), where

the prompts are simply fixed items in the Token Library. With this as a baseline, we compare against input-dependent prompting methods including a 2-layer MLP operating on the center  $10 \times 10$  pixels of an image, a ResNet10 at resolutions of  $64 \times 64$  and  $224 \times 224$ , as well as a ResNet18 at resolutions of  $224 \times 224$ . First, we observe that even a simple model such as a 2-layer MLP obtains a small performance benefit over the IIP. This might be explained by IIP being a strict subset of the input-dependent methods, as these could zero-out the input and instead supply constant prompts. The benefits of input-dependency is further demonstrated by using convolutional neural networks as backbones with gains of up to +5.8% for CIFAR100 (77.9 vs. 72.1). Increasing input resolution from 64 to 224 also slightly improves +1.4% accuracy for CIFAR100. Finally, we observe that the overall performance saturates even when using a ResNet18 compared to the ResNet10, suggesting that the PGN can be lightweight and that the method automatically divides the labor between fine-grained recognition and providing prompts as cues.

**Token Library vs Direct Learning.** In Fig. 4 we study the approach of obtaining the prompts. We compare our token library (TL) with the more direct approach that obtains the prompts through a linear transformation of the image features. While we observe that both methods can be made to achieve similar performances, Fig. 4 clearly demonstrates the superiority of the TL in terms of parameter efficiency.

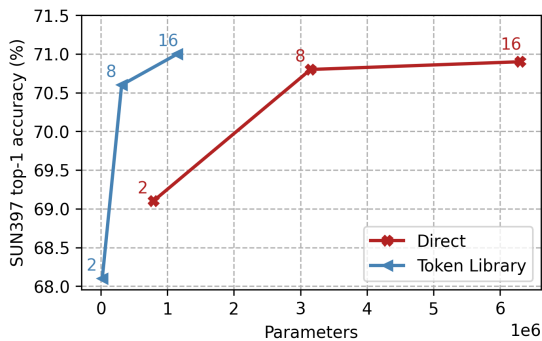


Figure 4: **Parameter efficiency.** We vary the number of generated tokens. A Token Library achieves higher performances at significantly less parameters compared to obtaining prompts directly. The library size used here is  $8 \times$  the number of prompts.

**Scaling to different frozen transformer models.** Finally, in Section 4.3, we explore the use of different pre-trained ViT backbones, from supervised training [13] and from self-supervised training using DINO [7]. First, we find that generally the performances are lower compared to those obtained from the CLIP backbone in Table 4. This means that adapting these networks is more challenging,

	DINO		ViT sup.	
	IIP	PGN	IIP	PGN
CIFAR100	13.2	<b>53.0</b>	18.8	<b>50.7</b>
SUN397	3.0	<b>19.2</b>	2.6	<b>6.3</b>
EuroSAT	85.8	<b>94.6</b>	91.9	<b>96.1</b>

Table 3: **Different pretrained models.** We compare PGN on two other ViT-B32 backbones from self-supervised DINO [7] and from supervised training [13]. Best results per backbone bolded.

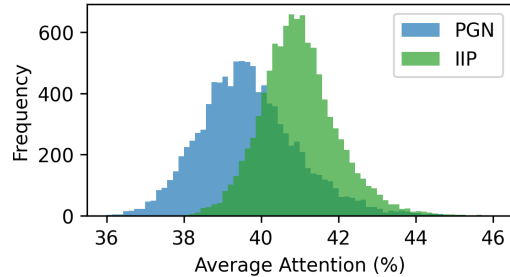


Figure 5: **Attention value histograms.** We show the individual attention values from the CLS token to the supplied prompts of PGN and IIP. We find that while PGN has an overall lower average attention, the input-dependency successfully yields a wider distribution in adapting the original model.

potentially owing to the vastly larger pretraining dataset of CLIP. Second, we find that both IIP and PGN struggle with adapting the backbones to the SUN397 dataset. This might be explained by: (i) the difference in image contents – while SUN contains scene images, the pretraining datasets of the supervised ViT and DINO are strongly object-centric [31] – and (ii) the relatively few image per class ( $\approx 190$ ). Third, we find that, as in the case of CLIP, the PGN approach vastly outperforms the baseline IIP approach in adapting these models to the datasets, e.g., showing gains of 40% for CIFAR100.

#### 4.4. Large-scale comparisons

Next, we compare PGNs to other input-based adaptation techniques on a wide range of vision datasets. Based on the findings of our ablations, we choose the ResNet10 as the PGN’s backbone, outputting 16 prompts from a Token Library of size 256 feeding into a pretrained CLIP ViT-B/32. The results are shown in Table 4 and are directly comparable to the concurrent work of Bahg *et al.* [2] on visual prompts (VP), from which we adapted the results of the first two rows. From Table 4, we first find that linear and full-finetuning and our method achieve the best performances on 4 out of 12 datasets each. However, when comparing the overall averaged accuracies, we find that our

Method	CIFAR100	CIFAR10	Flowers	Food	EuroSAT	SUN	UCF	SVHN	Pets	DTD	RESISC	CLEVR	Avg. $\Sigma$ params	
CLIP+TP	63.1	89.0	61.9	79.8	40.0	60.0	59.9	5.1	85.9	43.0	42.4	20.2	54.2	-
+ VP	75.3	94.2	70.3	78.9	96.4	60.6	66.1	88.4	85.0	57.1	84.5	81.4	78.2	0.94M
<b>+ PGN (ours)</b>	79.3	<b>96.1</b>	94.0	<b>82.5</b>	<b>98.0</b>	<b>70.9</b>	77.6	94.2	<b>91.5</b>	71.5	92.1	<b>95.1</b>	<b>86.9</b>	12.4M
Linear ft.	80.0	95.0	96.9	<b>84.6</b>	95.3	<b>75.0</b>	<b>83.3</b>	65.4	89.2	<b>74.6</b>	92.3	66.0	83.1	0.75M
full-ft.	<b>82.1</b>	95.8	<b>97.4</b>	80.5	97.9	64.0	80.9	<b>95.7</b>	88.5	72.3	<b>93.3</b>	94.4	<b>86.9</b>	1032M

Table 4: **Performance across 12 datasets.** We compare using CLIP with text prompting (TP), visual prompting (VP) [2], linear or full-finetuning (ft.) and our PGN method. The **green** shade indicates cases where PGN outperforms or matches full-finetuning performance. The bolding refers to best performance on a given dataset. We also report the additional number of parameters of the visual encoder for these 12 experiments for each configuration.

Method	EuroSAT	UCF	Pets	RESISC	Avg.	$\Delta$	$\Sigma$ params
CLIP+TP (I)	40.0	59.9	85.9	42.4	57.1	-	-
CLIP+TP (J)	4.4	59.7	85.8	47.7	49.4	-7.7%	-
+ PGN (I)	98.0	77.6	91.5	92.1	89.8	-	5M
+ PGN (J)	96.9	72.7	89.0	85.7	86.1	-3.7%	1M

Table 5: **Training a multi-dataset PGN.** Adapting and inferring jointly (J) over multiple datasets is compared to individual (I), per-dataset training and evaluation. While giving more text prompts (TP) for joint inference leads to a strong decrease in accuracy, joint training of the PGN retains a strong performance while reducing the number of additional parameters by 75%.

method achieves 86.9%, matching the performance of the full-finetuning adaptation, and surpassing both VP and linear finetuning by 8-3%. In the last column of Table 4, we show the number of additional parameters for adapting to each dataset. We find that our PGN method requires almost two orders of magnitude less parameters than full-finetuning, while retaining the same overall performance.

#### 4.5. Efficient Multi-dataset PGN

Encouraged by the comparisons of the previous section, we investigate whether PGNs can be made even more efficient, by training a PGN on multiple datasets at the same time. We retain the same setting as in Section 4.4 and train with batches that contain samples from the four datasets in Table 5. The model is thus forced to allocate the token library items in a manner that best supports this task, reducing the overall number of additionally adapted parameters by 75%. From Table 5, we find that despite this reduction in parameters, the overall performance only decreases by a small amount of 3.7%, despite the fact that the classification problem is now 193-way and thus much more difficult.

In Fig. 6 we show a *t*-SNE visualisation of the CLIP+PGN model that was trained jointly on four datasets. First, we find that the PGN learns features that are well-correlated with the domains. This is particularly interesting as the model did not receive any signal with regards to individual

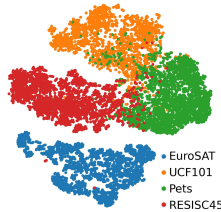


Figure 6: **Automatic domain discovery.** *t*-SNE visualisation of PGN outputs. PGN trained on a mixture of datasets automatically allocates the tokens in a manner that recovers the individual training domains.

items’ dataset origin, which shows that such a procedure could be used for adapting to mixed domain or unsorted datasets. Second, we observe that some domains contain images that have similar PGN outputs, notably between UCF and Pets. These are potentially explained by overlaps in depicted objects, *e.g.*, UCF contains classes such as “walking a dog”, while Pets contains multiple dog classes.

#### 4.6. Qualitative Analysis

From Table 1, we observed that the CLIP zero-shot and the PGN backbone model’s performance on their own are low with 63-64%. However, when combined, we reach performance increases of +15% yielding up to 79% on CIFAR100. In this section, we analyse how the simple mechanism behind PGN is allowing the combined model to achieve superior performances.

##### What do the individual Token Library items stand for?

To answer this question, we pass the validation sets through the trained PGN model and pick individual tokens that we wish to visualize. We then pick the top four input samples that have the highest softmax values for the selected item. The result is shown in Fig. 7 for three datasets. We find that while some tokens are fairly category specific, such as those for a tree or an apple, some cover much broader categories such as lighting conditions or even geometric structures. Note however that the PGN is not doing the heavy-lifting in terms of classifying the images by itself, as its output is not well-aligned with the ground-truth, as demonstrated in Fig. 3. It rather supplies the frozen transformer model with orthogonal information that helps the task.



Figure 7: **Token Library example items.** We show 4 samples that maximally activate one of three selected items in the token library for three datasets. Each row in the grid corresponds to one token library item. We find that the items can stand for whole objects such as apples and trees for CIFAR100, and also for lower level features such as light warmth or net structures as in UCF101.

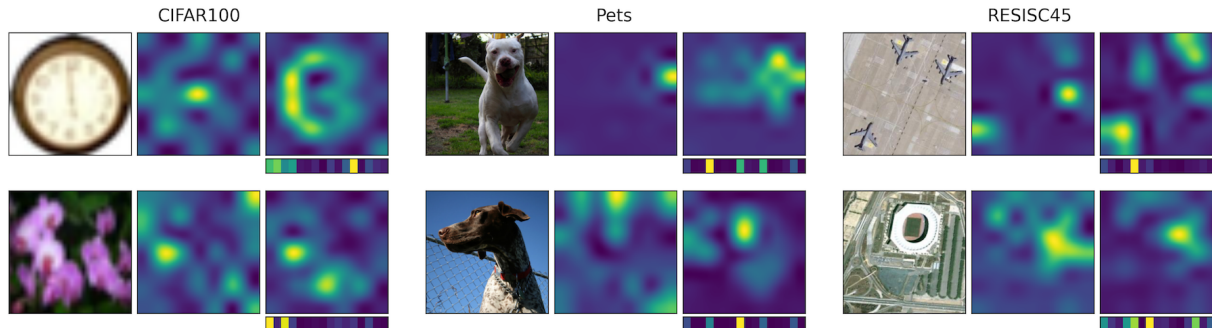


Figure 8: **Modification of CLS attention maps.** We show the attention map of the CLS token for various inputs (left) with the spatial patches for both the original CLIP model’s (middle) and the PGN-modified CLIP’s final layer (right). Below the PGN attention map, we show the attention to PGN’s additional prompts. We observe a clear modification of the attention map as well as the diverse activation patterns to the supplied tokens.

### How is the computation changed by PGN prompts?

Next, we analyse the effect of the PGN prompts to the internal computations of the frozen vision transformer. In Fig. 8, we visualize the CLS token’s attention map at the final layer of the transformer with or without our PGN. Despite showing the effect of the prompts on the *last* layer’s attention map, we still find a strong effect of the PGN’s additionally supplied prompts. While the effect is not interpretable for low-resolution datasets such as CIFAR, for Pets and Resisc we observe an increased focus on the foreground. We also show the attention values of the CLS to the 16 supplied prompts below the PGN-CLIP attention maps. A strong variance between images is seen, demonstrating that the method indeed learns and leverages the input-dependency of the prompts that are supplied to the frozen model.

## 5. Discussion and Conclusion

**Broader Impact.** The increasing size of large-scale pre-trained models have had a centralizing effect: only large companies and institutions have the resources to collect data and train on the required scale. One recently explored option to share the benefits of these models is to make it available for experimentation and inference through APIs. In

this work, we aim to empower future users of foundation model APIs by addressing the key limitation of restricted adaptability of models in this setting. However, we also recognize that our adaptation method could potentially be used by malicious actors for unintended purposes and vigilant monitoring of usages will remain important.

**Conclusion.** We propose Prompt Generator Network (PGN), a simple and effective framework for learning input-dependent visual prompts. Our method is parameter-efficient by leveraging a Token Library from which tokens are combined to yield the prompts using a lightweight network. Furthermore, it is compatible with recent developments that restrict access to model internals at inference, such as APIs or implementations on edge devices that require specialized hardware. We demonstrate that PGN can be used to adapt CLIP, surpassing previous methods and even matching and exceeding the results of full-finetuning of the visual encoder, despite requiring two orders of magnitude less number of adapted weights. Finally, we have demonstrated that PGN can be a scalable method for generic adaptation of frozen visual transformers by training them with a mixture of datasets.

## References

- [1] Yuki M. Asano, Christian Rupprecht, and Andrea Vedaldi. Self-labelling via simultaneous clustering and representation learning. In *ICLR*, 2020. 2
- [2] Hyojin Bahng, Ali Jahanian, Swami Sankaranarayanan, and Phillip Isola. Exploring visual prompts for adapting large-scale models. *arXiv:2203.17274*, 2022. 1, 2, 3, 5, 6, 7, 11, 12
- [3] Lukas Bossard, Matthieu Guillaumin, and Luc Van Gool. Food-101 – mining discriminative components with random forests. In *ECCV*, 2014. 4
- [4] Tom Brown, Benjamin Mann, Nick Ryder, Melanie Subbiah, Jared D Kaplan, Prafulla Dhariwal, Arvind Neelakantan, Pranav Shyam, Girish Sastry, Amanda Askell, et al. Language models are few-shot learners. *NeurIPS*, 33:1877–1901, 2020. 1, 2
- [5] Han Cai, Chuang Gan, Ligeng Zhu, and Song Han. Tinytl: Reduce memory, not parameters for efficient on-device learning. In *NeurIPS*, pages 11285–11297, 2020. 2
- [6] Mathilde Caron, Piotr Bojanowski, Armand Joulin, and Matthijs Douze. Deep clustering for unsupervised learning of visual features. In *ECCV*, pages 132–149, 2018. 2
- [7] Mathilde Caron, Hugo Touvron, Ishan Misra, Hervé Jégou, Julien Mairal, Piotr Bojanowski, and Armand Joulin. Emerging properties in self-supervised vision transformers. In *ICCV*, pages 9650–9660, 2021. 2, 4, 6
- [8] Ting Chen, Simon Kornblith, Mohammad Norouzi, and Geoffrey Hinton. A simple framework for contrastive learning of visual representations. *ICML*, 2020. 2
- [9] Gong Cheng, Junwei Han, and Xiaoqiang Lu. Remote sensing image scene classification: Benchmark and state of the art. *Proceedings of the IEEE*, 105(10):1865–1883, 2017. 4
- [10] Mircea Cimpoi, Subhansu Maji, Iasonas Kokkinos, Sammy Mohamed, and Andrea Vedaldi. Describing textures in the wild. In *CVPR*, pages 3606–3613, 2014. 4
- [11] Mostafa Dehghani, Josip Djolonga, Basil Mustafa, Piotr Padlewski, Jonathan Heek, Justin Gilmer, Andreas Steiner, Mathilde Caron, Robert Geirhos, Ibrahim Alabdulmohsin, et al. Scaling vision transformers to 22 billion parameters. *arXiv:2302.05442*, 2023. 1, 2
- [12] Jia Deng, Wei Dong, Richard Socher, Li-Jia Li, Kai Li, and Li Fei-Fei. Imagenet: A large-scale hierarchical image database. In *2009 IEEE Conference on Computer Vision and Pattern Recognition*, pages 248–255, 2009. 12
- [13] Alexey Dosovitskiy, Lucas Beyer, Alexander Kolesnikov, Dirk Weissenborn, Xiaohua Zhai, Thomas Unterthiner, Mostafa Dehghani, Matthias Minderer, Georg Heigold, Sylvain Gelly, Jakob Uszkoreit, and Neil Houlsby. An image is worth 16x16 words: Transformers for image recognition at scale. *ICLR*, 2020. 2, 3, 4, 6
- [14] Gamaleldin F Elsayed, Ian Goodfellow, and Jascha Sohl-Dickstein. Adversarial reprogramming of neural networks. *arXiv preprint arXiv:1806.11146*, 2018. 1, 2
- [15] Peng Gao, Shijie Geng, Renrui Zhang, Teli Ma, Rongyao Fang, Yongfeng Zhang, Hongsheng Li, and Yu Qiao. Clip-adapter: Better vision-language models with feature adapters. *arXiv:2110.04544*, 2021. 2
- [16] Priya Goyal, Mathilde Caron, Benjamin Lefauveux, Min Xu, Pengchao Wang, Vivek Pai, Mannat Singh, Vitaliy Liptchinsky, Ishan Misra, Armand Joulin, et al. Self-supervised pre-training of visual features in the wild. *arXiv:2103.01988*, 2021. 1
- [17] Tengda Han, Weidi Xie, and Andrew Zisserman. Memory-augmented dense predictive coding for video representation learning. In *ECCV*, pages 312–329. Springer, 2020. 4
- [18] Kaiming He, Haoqi Fan, Yuxin Wu, Saining Xie, and Ross Girshick. Momentum contrast for unsupervised visual representation learning. In *CVPR*, pages 9729–9738, 2020. 2
- [19] Kaiming He, Xiangyu Zhang, Shaoqing Ren, and Jian Sun. Deep residual learning for image recognition. In *CVPR*, pages 770–778, 2016. 4
- [20] Patrick Helber, Benjamin Bischke, Andreas Dengel, and Damian Borth. Eurosat: A novel dataset and deep learning benchmark for land use and land cover classification. *IEEE Journal of Selected Topics in Applied Earth Observations and Remote Sensing*, 2019. 4
- [21] Dan Hendrycks, Steven Basart, Norman Mu, Saurav Kadavath, Frank Wang, Evan Dorundo, Rahul Desai, Tyler Zhu, Samyak Parajuli, Mike Guo, Dawn Song, Jacob Steinhardt, and Justin Gilmer. The many faces of robustness: A critical analysis of out-of-distribution generalization. *ICCV*, 2021. 12
- [22] Dan Hendrycks, Kevin Zhao, Steven Basart, Jacob Steinhardt, and Dawn Song. Natural adversarial examples. *arXiv preprint arXiv:1907.07174*, 2019. 12
- [23] Neil Houlsby, Andrei Giurgiu, Stanislaw Jastrzebski, Bruna Morrone, Quentin De Laroussilhe, Andrea Gesmundo, Mona Attariyan, and Sylvain Gelly. Parameter-efficient transfer learning for nlp. *ICML*, 2019. 2
- [24] Chao Jia, Yinfei Yang, Ye Xia, Yi-Ting Chen, Zarana Parekh, Hieu Pham, Quoc Le, Yun-Hsuan Sung, Zhen Li, and Tom Duerig. Scaling up visual and vision-language representation learning with noisy text supervision. In *ICML*, pages 4904–4916. PMLR, 2021. 1, 2
- [25] Menglin Jia, Luming Tang, Bor-Chun Chen, Claire Cardie, Serge Belongie, Bharath Hariharan, and Ser-Nam Lim. Visual prompt tuning. *ECCV*, 2022. 2, 3
- [26] Justin Johnson, Bharath Hariharan, Laurens Van Der Maaten, Li Fei-Fei, C Lawrence Zitnick, and Ross Girshick. Clevr: A diagnostic dataset for compositional language and elementary visual reasoning. In *CVPR*, pages 2901–2910, 2017. 4
- [27] Chen Ju, Tengda Han, Kunhao Zheng, Ya Zhang, and Weidi Xie. Prompting visual-language models for efficient video understanding. In *ECCV*, 2022. 2, 3
- [28] Eliska Klobertanz, Jin Tian, and Wei Le. An improved (adversarial) reprogramming technique for neural networks. In *International Conference on Artificial Neural Networks*, pages 3–15. Springer, 2021. 1, 2
- [29] Alex Krizhevsky, Geoffrey Hinton, et al. Learning multiple layers of features from tiny images. *Technical Report*, 2009. 4
- [30] Ankit Kumar, Ozan Irsoy, Peter Ondruska, Mohit Iyyer, James Bradbury, Ishaan Gulrajani, Victor Zhong, Romain Paulus, and Richard Socher. Ask me anything: Dynamic memory networks for natural language processing. In *ICML*, pages 1378–1387. PMLR, 2016. 4
- [31] Alina Kuznetsova, Hassan Rom, Neil Alldrin, Jasper Ui-

- jlings, Ivan Krasin, Jordi Pont-Tuset, Shahab Kamali, Stefan Popov, Matteo Mallocci, Alexander Kolesnikov, et al. The open images dataset v4. *IJCV*, pages 1956–1981, 2020. 6
- [32] Brian Lester, Rami Al-Rfou, and Noah Constant. The power of scale for parameter-efficient prompt tuning. *EMNLP*, 2021. 3
- [33] Xiang Lisa Li and Percy Liang. Prefix-tuning: Optimizing continuous prompts for generation. *ACL*, 2021. 2, 3
- [34] Yuval Netzer, Tao Wang, Adam Coates, Alessandro Bis-sacco, Bo Wu, and Andrew Y Ng. Reading digits in natural images with unsupervised feature learning. *NeurIPS Workshop on Deep Learning and Unsupervised Feature Learning*, 2011. 4
- [35] Maria-Elena Nilsback and Andrew Zisserman. Automated flower classification over a large number of classes. In *Sixth Indian Conference on Computer Vision, Graphics & Image Processing*, pages 722–729. IEEE, 2008. 4
- [36] Omkar M Parkhi, Andrea Vedaldi, Andrew Zisserman, and CV Jawahar. Cats and dogs. In *CVPR*, pages 3498–3505. IEEE, 2012. 4
- [37] Jonas Pfeiffer, Andreas Rücklé, Clifton Poth, Aishwarya Kamath, Ivan Vulić, Sebastian Ruder, Kyunghyun Cho, and Iryna Gurevych. Adapterhub: A framework for adapting transformers. *EMNLP*, 2020. 2
- [38] Alec Radford, Jong Wook Kim, Chris Hallacy, Aditya Ramesh, Gabriel Goh, Sandhini Agarwal, Girish Sastry, Amanda Askell, Pamela Mishkin, Jack Clark, Gretchen Krueger, and Ilya Sutskever. Learning transferable visual models from natural language supervision. *ICML*, 2021. 1, 2, 4, 12
- [39] Alec Radford, Jeffrey Wu, Rewon Child, David Luan, Dario Amodei, and Ilya Sutskever. Language models are unsuper-vised multitask learners. *OpenAI Technical Report*, 2019. 2
- [40] Benjamin Recht, Rebecca Roelofs, Ludwig Schmidt, and Vaishal Shankar. Do imagenet classifiers generalize to imagenet? In *International conference on machine learning*, pages 5389–5400. PMLR, 2019. 12
- [41] Khurram Soomro, Amir Roshan Zamir, and Mubarak Shah. Ucf101: A dataset of 101 human actions classes from videos in the wild. *arXiv preprint arXiv:1212.0402*, 2012. 4
- [42] Sainbayar Sukhbaatar, Jason Weston, Rob Fergus, et al. End-to-end memory networks. *NeurIPS*, 28, 2015. 4
- [43] Ashish Vaswani, Google Brain, Noam Shazeer, Niki Parmar, Jakob Uszkoreit, Llion Jones, Aidan N Gomez, Łukasz Kaiser, and Illia Polosukhin. Attention is all you need. *NeurIPS*, 2017. 2
- [44] Haohan Wang, Songwei Ge, Zachary Lipton, and Eric P Xing. Learning robust global representations by penalizing local predictive power. In *Advances in Neural Information Processing Systems*, pages 10506–10518, 2019. 12
- [45] Zifeng Wang, Zizhao Zhang, Sayna Ebrahimi, Ruoxi Sun, Han Zhang, Chen-Yu Lee, Xiaoqi Ren, Guolong Su, Vincent Perot, Jennifer Dy, et al. Dualprompt: Complementary prompting for rehearsal-free continual learning. In *Computer Vision–ECCV 2022: 17th European Conference, Tel Aviv, Israel, October 23–27, 2022, Proceedings, Part XXVI*, pages 631–648. Springer, 2022. 4
- [46] Zifeng Wang, Zizhao Zhang, Chen-Yu Lee, Han Zhang, Ruoxi Sun, Xiaoqi Ren, Guolong Su, Vincent Perot, Jennifer Dy, and Tomas Pfister. Learning to prompt for continual learning. In *Proceedings of the IEEE/CVF Conference on Computer Vision and Pattern Recognition*, pages 139–149, 2022. 4
- [47] Mitchell Wortsman, Gabriel Ilharco, Jong Wook Kim, Mike Li, Simon Kornblith, Rebecca Roelofs, Raphael Gon-tijo Lopes, Hannaneh Hajishirzi, Ali Farhadi, Hongseok Namkoong, et al. Robust fine-tuning of zero-shot models. In *CVPR*, 2022. 2
- [48] Zhirong Wu, Yuanjun Xiong, Stella X Yu, and Dahua Lin. Unsupervised feature learning via non-parametric instance discrimination. In *CVPR*, pages 3733–3742, 2018. 2
- [49] Jianxiong Xiao, James Hays, Krista A Ehinger, Aude Oliva, and Antonio Torralba. Sun database: Large-scale scene recognition from abbey to zoo. In *CVPR*, pages 3485–3492. IEEE, 2010. 4
- [50] Yuan Yao, Ao Zhang, Zhengyan Zhang, Zhiyuan Liu, Tat-Seng Chua, and Maosong Sun. Cpt: Colorful prompt tuning for pre-trained vision-language models. *arXiv:2109.11797*, 2021. 2
- [51] Elad Ben Zaken, Shauli Ravfogel, and Yoav Goldberg. Bitfit: Simple parameter-efficient fine-tuning for transformer-based masked language-models. *ACL*, 2021. 2
- [52] Jeffrey O Zhang, Alexander Sax, Amir Zamir, Leonidas Guibas, and Jitendra Malik. Side-tuning: a baseline for network adaptation via additive side networks. In *ECCV*, pages 698–714. Springer, 2020. 2
- [53] Renrui Zhang, Rongyao Fang, Peng Gao, Wei Zhang, Kunchang Li, Jifeng Dai, Yu Qiao, and Hongsheng Li. Tip-adapter: Training-free clip-adapter for better vision-language modeling. *arXiv:2111.03930*, 2021. 1, 2
- [54] Kaiyang Zhou, Jingkang Yang, Chen Change Loy, and Ziwei Liu. Conditional prompt learning for vision-language models. *CVPR*, 2022. 2
- [55] Kaiyang Zhou, Jingkang Yang, Chen Change Loy, and Ziwei Liu. Learning to prompt for vision-language models. *IJCV*, 2022. 2, 3

## A. Appendix

### B. Details of the Datasets

Table 6 gives an overview of the downstream datasets used for the evaluation of our method, including the text prompt templates used to generate classifiers for CLIP.

Dataset	#Train	# Val.	# Test	Classes	Text Prompt
CIFAR100	50K	-	10K	100	“This is a photo of a { }”
CIFAR10	50K	-	10K	10	“This is a photo of a { }”
Flowers102	4K	1.6K	2.5K	102	“This is a photo of a { }”
Food101	50K	20K	30.3K	101	“This is a photo of a { }”
EuroSAT	13.5K	5.4K	8.1K	10	“This is a photo of a { }”
SUN397	15.9K	4K	19.9K	397	“This is a photo of a { }”
UCF101	7.6K	1.9K	3.7K	101	“This is a photo of a { }”
SVHN	73.3K	-	26K	10	“This is a photo of a { }”
OxfordPets	2.9K	736	3.6K	37	“This is a photo of a { }”
DTD	2.8K	1.1K	1.6K	47	“This is a photo of a { }”
Resisc45	18.9K	6.3K	6.3K	45	“This is a photo of a { }”

Table 6: Description of the datasets and the corresponding text prompt used for CLIP. Table adapted from [2].

Table/Figure	Epochs	Number of prompts	TL Size	PGN resolution
Table 1	1000*	16	256	224 × 224
Table 2	500	8	64	64 × 64
Table 3	500	16	256	224 × 224
Table 4	1000	16	256	224 × 224
Table 5	500	16	256	224 × 224
Figure 2	1000	16	256	224 × 224
Figure 3	500	8	64	64 × 64
Figure 4	1000	16	256	224 × 224
Figure 5	1000	16	256	224 × 224
Figure 6	1000	16	256	224 × 224
Figure 7	1000	16	256	224 × 224

Table 7: Experimental settings for each of our tables and figures. (\*) In the main paper Table 1, the reported numbers for VP do not come from our own experimentation, hence our settings do not apply.

### C. Additional Experimental Settings

**Training Details.** In Table 7, we show the training details of the experiments in the main paper.

**Architectures.** In Table 8, we show the details of ResNet10 architectures.

**Feature Similarities Computation.** For Figure 3 in the main paper, we embed the validation set of CIFAR-100 using the three visual encoders of PGN (only), CLIP, and PGN+CLIP. For this we cluster the features into 100 clusters using k-means. After this, the representations can be easily compared with each other using the normalised mutual information score.

stage	specification	output sizes $H \times W \times C$
input data	-	$224^2 \times 3$
conv <sub>1</sub>	$7 \times 7, 16$ stride 2, 2	$112^2 \times 16$
pool <sub>1</sub>	$3 \times 3, 16$ stride 2, 2	$56^2 \times 16$
res <sub>2</sub>	$3 \times 3, 16$ $3 \times 3, 16$ × 1	$56^2 \times 16$
res <sub>3</sub>	$3 \times 3, 32$ $3 \times 3, 32$ × 1	$28^2 \times 32$
res <sub>4</sub>	$3 \times 3, 64$ $3 \times 3, 64$ × 1	$14^2 \times 64$
res <sub>5</sub>	$3 \times 3, 128$ $3 \times 3, 128$ × 1	$7^2 \times 128$
pool <sub>2</sub>	$7 \times 7, 128$ stride 1, 1	$1^2 \times 128$

Table 8: The structure of ResNet10, which is modified from ResNet18 to be more light-weight. Modifications are marked in red. Note that the final classification layer is omitted.

### D. Details of Feature Similarity Analysis

In the NMI analysis in Figure 3 and Sec. 4.2 of the main paper, we measure the pairwise alignment between the outputs of the visual encoders we use and the ground truth. These are: the frozen CLIP model’s visual encoder that outputs CLS embedding, the trained PGN model that outputs prompts (the  $\mathbf{h}_V$  in Eqn. 4), and the combined CLIP+PGN model which uses PGN prompts to modify CLIP’s visual encoder’s outputs (that outputs CLS embedding after CLIP). For this, we apply k-means clustering to the set of embeddings generated by each encoder individually, setting k equal to the number of ground-truth classes. For our experiment, we use the full CIFAR100 test split. This yields a set of 3 pseudo labelings of the dataset. After combination with the ground-truth labels, we can make 6 pairwise comparisons and calculate the normalised mutual information, which measures a generalized correlation between labelings. The results are shown in Table 9.

NMI	GT	PGN	CLIP	PGN+CLIP
GT	100	29.5	58.1	<b>70.1</b>
PGN		100	27.5	33.8
CLIP			100	61.2
PGN+CLIP				100

Table 9: Normalized Mutual Information (NMI) score in %.

## E. Large-scale comparisons

In Table 5 in the main paper, the results for linear are adopted from the original CLIP paper [38], whereas the results for full finetuning are taken from VP [2].

## F. Additional Experiments

**Comparison between linear and non-linear layer.** In Table 10 we evaluate replacing the final linear layer of  $g_\theta$  with a MLP with 1 hidden layer, which allows for a nonlinear mapping between image features and the logits that give rise to the combination coefficients in Eqn. 4. No significant performance gain is observed.

Type	CIFAR100	SUN397
Linear	77.9	<b>70.5</b>
MLP	<b>78.2</b>	70.4

Table 10: Feature projection layer type.

**Unfreezing the classification layer.** So far, we have utilized CLIP’s text prompts (TP) to generate the fixed weights of a linear classifier. In Table 11, we compare this approach to a trainable classifier, which takes the TP weights as a starting point.

Cls.	CIFAR100	SUN397
TP	79.3	70.9
+ SGD	79.3	70.3

Table 11: Training a linear layer in addition to PGN.

**Experiments on Robustness.** We evaluate the robustness of PGNs by training for 100 epochs on ImageNet [12] and evaluating on four ImageNet variations (ImageNet-A [22], ImageNet-R [21], Imagenet-V2 [40] and Imagenet-Sketch [44]). For these experiments, we use identical PGN settings as in Table 5 in the original paper. The results are shown in Table 12 and compared to the case of linear finetuning on the same, frozen CLIP backbone (ViT-B/32). We see

Method	ImageNet	A	R	V2	Sketch
PGN	66.0	22.8	62.5	56.7	36.5
LP	67.0	10.6	38.1	1.0	36.1

Table 12: Evaluation accuracies on 4 robustness benchmarks. We compare adaptation with a PGN to linear finetuning (LP).

that the PGN outperforms linear finetuning on all robustness benchmark, despite being comparable in terms of its performance on the upstream dataset.

## G. Version History

**Version-2 (updated in March 2023):**

- Rewrite: clearer differentiation between input-only vs deep prompting/learning methods
- Added: prompt inversion trick for input-only prompting during inference
- Added: experiments in which we evaluated the robustness of PGN on common benchmarks